

PARTICLE SWARM OPTIMIZATION-BASED DETERMINATION OF HYDRAULIC JUMP LOCATION IN SLUICE GATE FLOWS

^{1,*} Ali YILDIZ ⁽¹⁾, ^{2,*} Volkan YILMAZ ⁽¹⁾

¹ Konya Technical University, Engineering and Natural Sciences Faculty, Civil Engineering Department, Konya, TÜRKİYE

¹ayildiz@ktun.edu.tr, ²vyilmaz@ktun.edu.tr

Highlights

- Locations of the hydraulic jump for 5 gate openings were recorded for 96 experiments
- Particle Swarm Optimization (PSO) used to estimate position of hydraulic jump
- PSO algorithm produced more successful solutions with the linear model

Graphical Abstract



Flowchart of the experimental study and PSO analysis

ISSN: 2667-8055 (Electronic) DOI: 10.36306/konjes.1652389



PARTICLE SWARM OPTIMIZATION-BASED DETERMINATION OF HYDRAULIC JUMP LOCATION IN SLUICE GATE FLOWS

^{1,*} Ali YILDIZ ⁽¹⁾, ^{2,*} Volkan YILMAZ ⁽¹⁾

¹ Konya Technical University, Engineering and Natural Sciences Faculty, Civil Engineering Department, Konya, TÜRKİYE

¹ ayildiz@ktun.edu.tr, ² vyilmaz@ktun.edu.tr

(Received: 06.03.2025; Accepted in Revised Form: 17.06.2025)

ABSTRACT: The hydraulic jump is a critical phenomenon in open channel hydraulics, and understanding its behavior is essential for the design and safety of hydraulic structures. In this study, 96 experiments were conducted using five different gate openings to model the location of hydraulic jumps in an open channel. The Particle Swarm Optimization (PSO) algorithm, a metaheuristic optimization technique, was employed to develop both linear and nonlinear predictive models. Experimental data from gate openings (e) of 2.5 cm, 3.5 cm, 4 cm, and 5 cm were used to train the models, while data from a e=6 cm gate opening were used for testing. The results demonstrated that the PSO algorithm effectively modeled the hydraulic jump location, yielding high accuracy and consistency with experimental observations. Model performance was evaluated using the Coefficient of Determination (R2), Nash-Sutcliffe Efficiency (NSE), and Mean Squared Error (MSE). The linear model outperformed the nonlinear model, achieving NSE = 0.954, $R^2 = 0.983$, and MSE = 0.022. Furthermore, the upstream total head (H) and gate opening (e) were identified as the most influential parameters affecting the hydraulic jump location.

Keywords: Open Channel Hydraulics, Sluice Gate, Hydraulic Jump, Particle Swarm Optimization (PSO)

1. INTRODUCTION

Sluice gates regulate water levels in reservoirs and open channels, maintain water level at maximum, capture floating objects, and manage the controlled release of excess water to downstream. After sudden rainfall, the opening (e) under the sluice gates is adjusted to regulate discharge (Q) and to prevent sudden floods passing to the downstream side by providing controlled release of water [1]. The flow passing under the gate in supercritical flow regime (F₁>1) may cause scour at the end of the spillway and on the downstream side of the river, so the energy of the flow must be reduced before it passes to the downstream side [2]. Energy dissipation can be achieved through the energy loss (ΔE) that occurs during the hydraulic jump. Hydraulic jump is created by the flow under the gate in supercritical regime (F_r>1) in the free flow condition and passing to the subcritical regime (F_r<1) [3]. While hydraulic jump sometimes occurs naturally, in some cases, energy dissipation structures are constructed on the downstream side of the channel to provide hydraulic jump formation and increase energy loss (ΔE) and to ensure the transition of flow to the subcritical regime [4]. Energy dissipating structures and pools are designed in various ways based on the Froude number (F_r) and the approach velocity (V₁) of the supercritical flow. Blocks, barriers, and thresholds are installed within these pools to aid in energy dissipation [5]. The hydraulic jump is intended to be formed in a designated location inside the energy dissipation pools [6]. An uncontrolled hydraulic jump occurring outside the energy dissipation pools may pose a danger to the riverbed, open channels and surrounding hydraulic structures [7]. The hydraulic jump location must be known exactly so that the hydraulic jump does not damage the surrounding structures and the channel it is located in.

In the first studies on hydraulic jump, researchers tried to explain the behavior of hydraulic jump with momentum equations [8], [9]. Levy et al. [10] investigated the amount of energy loss (ΔE) and the mixing of chemicals into water in their hydraulic jump experiments. Rouse et al. [11] investigated the

average velocities and turbulences patterns during the jump experimentally and theoretically to explain the behavior of hydraulic jump. Silvester [12] found semi-empirical analytical solutions for conjugate depth, energy loss rate ($\%\Delta E$) and jump length (L_J) for different Froude numbers (F_r) in horizontal rectangular, triangular, parabolic, circular and trapezoidal channels. Rajaratnam and Subramanya [13] obtained a generalized water surface profile for hydraulic jumps formed in smooth and rectangular open channels. Hager and Wanoschek [14] determined the surface profiles and velocity distributions of hydraulic jump in a triangular channel and compared the results with hydraulic jumps in a rectangular channel. Gharangik and Chaudhry [15] used Boussinesq equations to create a two-dimensional numerical model of hydraulic jump in a rectangular channel with low bed slope (θ) . Ead et al. [16] experimentally investigated hydraulic jumps in an open channel with different bottom roughness for Froude numbers (F₁) from 4 to 10. Habibzadeh et al. [17] derived the discharge coefficient (C₄) formula using theoretical methods to calculate the energy loss (ΔE) under rectangular sluice gates in submerged and free flow conditions. The accuracy of the formula was tested using experimental studies in the literature and it was seen that the energy loss (ΔE) in sluice gates is mainly affected by the geometry of the gate. Kim et al. [18] conducted experiments to examine the characteristic features of hydraulic jumps formed by fixed weirs and movable sluice gates and to compare their effects on energy dissipation (ΔE). Movahed et al. [19] et al. developed an semi analytical formula to find the length of the hydraulic jump (L_J) using 387 experimental data points. Simsek et al. [20] examined the length of the hydraulic jump (L_J) formed in a stilling basin with two different bed slopes (θ) and six different Froude numbers (F_r) . They found that as the Froude number (F_r) decreases, the length of the hydraulic jump (L_I) increases.

In recent years, researchers have been using artificial intelligence techniques for hydraulic jumps modeling. Naseri and Othman [21] calculated the length of the hydraulic jump (L_J) formed in a rectangular channel using an artificial neural network (ANN) model with the Levenberg-Marquardt (LM) and gradient descent with momentum and adaptive learning rule back propagation (BP) algorithms. Omid et al. [22] used ANN models to model the sequent depth ratio (y2/y1) and length of hydraulic jump (L_J), evaluating 16 configurations with different numbers of hidden layers and neurons. In the study, 611 experimental data points were collected for gradually expanding jumps in rectangular and trapezoidal channels. Karbasi and Azamathulla [23] used the Gene Expression Programming (GEP) method to predict the jump length ratio (L₁/y₁) and sequent depth ratio (y₂/y₁) of the hydraulic jump formed on a rough channel bed. The GEP model, created with 491 experimental data points, was evaluated for accuracy and performance along with ANN and SVR models. Karbasi [24] used the teaching-learning-based optimization (TLBO) algorithm to predict the length of a classical hydraulic jump (L_I). For the TLBO model, 167 experimental data points were used, and the algorithm was applied to four different regression forms (linear, quadratic, exponential, and power). Gul et al. [25] predicted the relative jump length (L_j/y₁) and characteristics such as sequent depth ratios (y₂/y₁) of the hydraulic jump formed in a suddenly expanding stilling basin using a hybrid extreme learning machine (ELM). In their study, Froude Number (F1), expansion ratio (B=b1/b2), and relative sill height (S=s/y1) were given as inputs, and sequent depth ratio (Y=y2/y1) and LJ/y1 values were predicted. To hybridize the ELM, metaheuristic algorithms such as the imperialist competitive algorithm (ICA), firefly algorithm (FA), and particle swarm optimization (PSO) were used.

As can be seen from the literature review, most of the studies in the literature focus on determining the length of the hydraulic jump and the depths before and after the jump. There are not many studies in literature aimed at determining the location of the hydraulic jump. In this study, the location of free hydraulic jump formed by the flow passing under the gate in a rectangular open channel with a constant width experimentally determined and modeled with ANN. In experimental studies, 5 different gate openings (e_1 =2.5 cm, e_2 =3.5 cm, e_3 =4 cm, e_4 =5 cm, and e_5 =6 cm) were used, and a total of 96 experimental data were collected. The locations of the hydraulic jumps were determined for varying gate openings (e_1) and discharge values (Q). The most important parameters affecting the location of the hydraulic jump (e_1) are the total head on the upstream side (H), the velocity (e_1), the flow depths before the jump (e_2) and after the jump (e_2) [26]. Therefore, parameters H, e_1 , e_2 , and e_3 were considered as input parameters

in the Particle Swarm Optimization (PSO) algorithm, and the location of the hydraulic jump (L) was attempted to be predicted. The results obtained from the PSO algorithm were compared with the experimental data to test the accuracy of the mathematical model.

2. MATERIAL AND METHODS

2.1. Sluice gate and Hydraulic jump

Sluice gates provide a rectangular bottom opening from the front view through which water can pass. The discharge (Q) passing under the sluice gate varies depending on the opening (e) under the sluice gate and the total head on the upstream side (H). The flow passing under a sluice gate can be in two conditions: free flow or submerged flow.

<u>1- Free flow condition:</u> After the flow passes under the gate, it is in supercritical regime and open to the atmosphere (Figure 1(a)). The flow depth (y_1) is smaller than the gate opening (e). If the flow on the downstream side is in subcritical regime, hydraulic jump may occur away from the gate resulting in energy dissipation and head loss (ΔE).

2-Submerged flow condition: After the flow passes under the gate, it is not open to the atmosphere and the hydraulic jump caused by the flow occurs adjacent to the downstream surface of the sluice gate. The flow depth (y_2) is greater than the gate opening (e) (Figure 1(b)). A free hydraulic jump does not form; instead, a submerged hydraulic jump occurs, accompanied by head loss (ΔE) due to intense turbulence and backflow effects. The free and submerged flow conditions passing under the sluice gate are shown in Figure 1. The total upstream water head (H) behind the gate is equal to the sum of the piezometric depth (h) and the velocity head ($V^2/2 \times g$). ($H = h + V^2/2 \times g$)

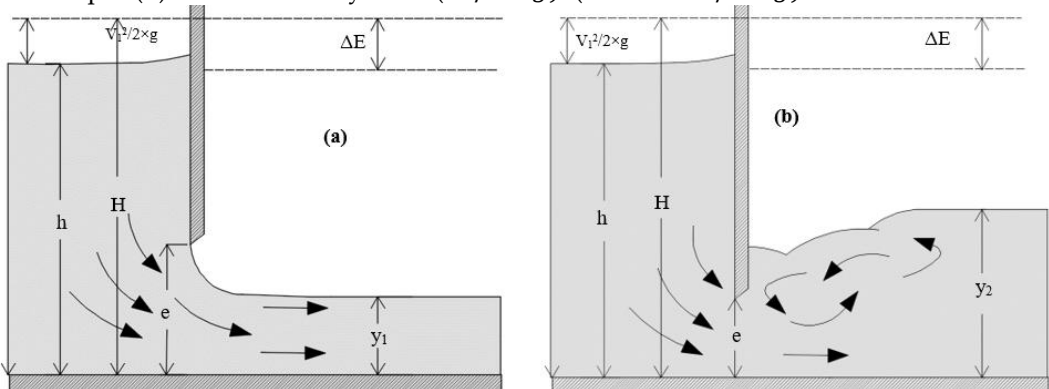


Figure 1. Free (a) and submerged (b) flow conditions passing under the sluice gate

The discharge of the flow passing under the sluice gate is determined by the following Equation (1);

$$Q = C_d * e * b * \sqrt{2 * g * H}$$
Where;
(1)

Q: Discharge (m³/s)

C_d: Discharge Coefficiente: Gate opening (m)

b : Gate width (m)

H: Upstream total head (m)

The free or submerged condition of the flow passing under a sluice gate can be determined from Figure 2, depending on the upstream head (H) and downstream (y₂) water levels. Depending on whether the value obtained from the H/e and y₂/e ratios remains above or below the curve, it is determined whether the flow will be submerged or free flowing.

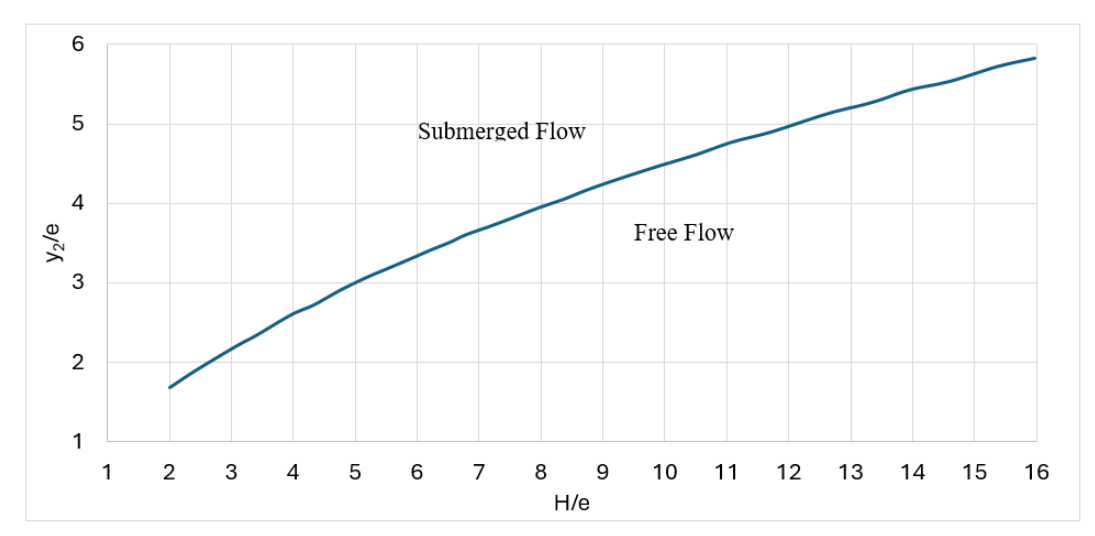


Figure 2. Determination of the flow type depending on the H/e and y₂/e ratios. [13].

In the case of free flow, the discharge coefficient (C_d) depends on the upstream water head (H) and the gate opening (e), while in the submerged flow case, the discharge coefficient (C_d) depends on the downstream water level (y_2) and the gate opening (e). In addition, the discharge coefficient (C_d) values are read from a single curve in the free flow case, while the discharge coefficient (C_d) is read from different curves in the submerged flow case depending on the degree of submergence. The variation of the discharge coefficient (C_d) depending on the H/e and y_2 /e ratios is shown in Figure 3.

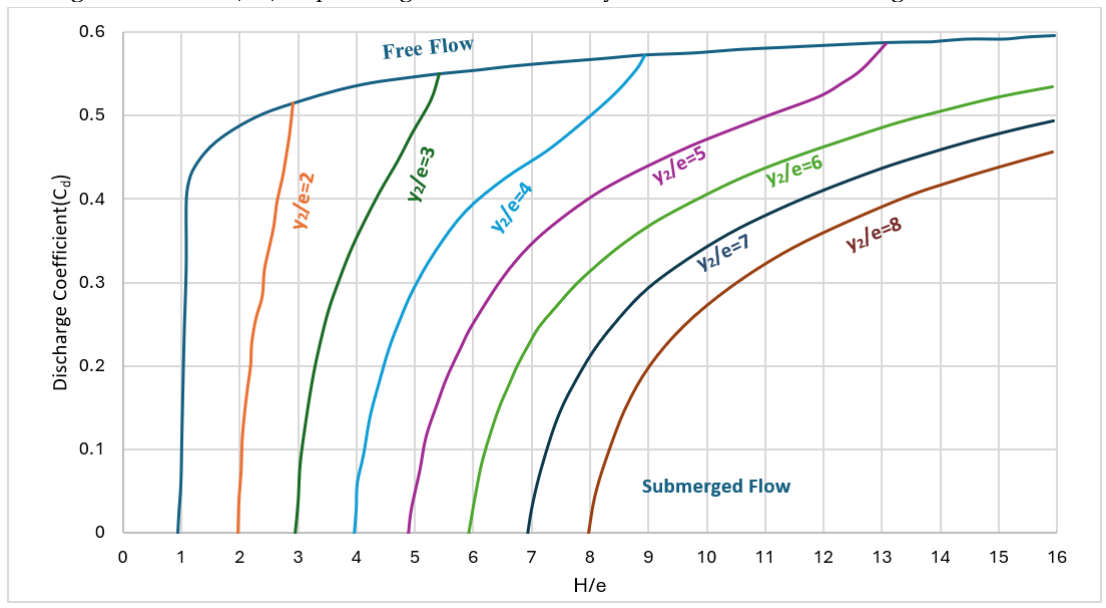


Figure 3. Determination of the discharge coefficient (Cd) depending on the H/e and y₂/e ratios for the submerged and free flow conditions [27]

If the depth of a flow changes significantly over a short distance in an open channel, it is called rapidly varying flow (RVF) and if it changes more slowly over a long distance, it is called gradually varying flow (GVF). Hydraulic jump is classified as rapidly varying flow (RVF) and occurs when the flow is exposed to turbulence as it passes from the supercritical (Fr>1) to the subcritical regime (Fr<1) (Figure 4). The flow regime in open channels is determined by the Froude number. The Froude number is calculated from the ratio of inertial forces to gravitational forces and is formulated as $F_r = V/\sqrt{g*y}$. Here, V is the velocity, g is the acceleration of gravity and y is the hydraulic depth (for rectangular channels). When inertial forces are greater than the gravitational forces (Fr>1), flow is called the

supercritical. When inertial forces are less than the gravitational forces (Fr<1), flow is called the subcritical. Hydraulic jumps occur in two ways, submerged and free, depending on the state of the flow [28].

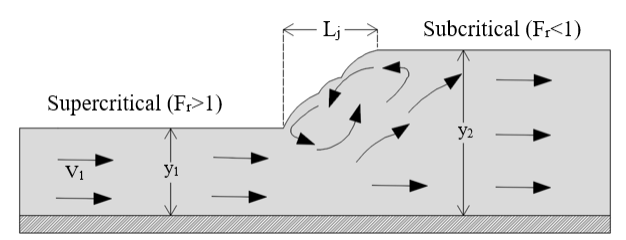


Figure 4. Hydraulic jump

Hydraulic jumps pose a great danger when they occur uncontrolled in open channels because large forces are generated during the jump and the depth of the flow suddenly increases. A controlled hydraulic jump is beneficial in terms of aeration and energy dissipation (ΔE). In submerged hydraulic jumps, in addition to the fact that the supercritical and subcritical parts of the flow cannot be determined exactly, the amount of energy to be broken cannot be calculated with the formula used in free jump. Calculations of submerged hydraulic jumps are generally made with experimental and numerical studies. High-energy flow from the spillway crest can lead to erosion in the riverbed. Strong turbulences can damage the material on the river bed and cause abrasions. Subjecting the flow from the spillway in the flood regime to a controlled hydraulic jump will reduce the energy of the flow and make it easier and safer to transport water. The flow depth before (y_1) and after (y_2) the hydraulic jump and the total energy loss (ΔE) are calculated with Equations (2) and (3).

$$y_2 = \frac{y_1}{2} * (\sqrt{1 + 8 * Fr_1^2} - 1) \tag{2}$$

$$\Delta E = \frac{(y_2 - y_1)^3}{4^* y_1 * y_2} \tag{3}$$

Where; y_1 is the flow depth before the hydraulic jump, y_2 is the flow depth after the hydraulic jump, $F_{r,1}$ is the Froude number in the supercritical regime and ΔE is the total amount of energy loss in the hydraulic jump.

2.2. Experimental Setup

In this study, experiments were conducted on an open channel system to investigate the alternating position (L) of the hydraulic jump created by a flow passing under the sluice gate depending on the discharge (Q) and the gate opening (e) (Figure 5). The open channel system where the physical experiment setups were prepared is 6.5 m long, 0.5 m deep and 0.6 m wide. The walls and bed of the open channel are made of 1.2 cm thick laminated tempered glass. The bed slope of the open channel system is 0.7 %. The flow in the open channel system is provided by two reservoirs between which the channel is placed. Two parallel connected pumps take water from the downstream reservoir and send it to the upstream reservoir through pipes. After water fills the upstream reservoir and reaches its maximum level, it overflows into the open channel system and is eventually discharged into the downstream reservoir at the end of the channel. The amount of discharge that the pumps will provide to the pipe is adjusted by the frequency converter that controls the pumps. Discharge is measured with an ultrasonic flow meter with a sensitivity of 0.01 l/s, placed on the main pipe.





Figure 5. Experimental setup

In the experiments, 5 different gate openings ($e_1=2.5$ cm, $e_2=3.5$, $e_3=4$ cm, $e_4=5$ cm and $e_5=6$ cm) were used (Figure 6). The sluice gates were manufactured from 1 cm thick plexiglas material. The bottom edge of the sluice gates where the water passes has a flat crest shape and its thickness is equal to the gate thickness of 1 cm. Flow depth measurements were made with a limnimeter at 3 different points in open channel, which are the total upstream water depth behind the sluice gate (h), the water depth before the jump (y_1) and the water depth after the jump (y_2). Also the distance of the hydraulic jump to the gate (L) was measured. The measured parameters and the total number of measurements are shown in Table 1.

Table 1. Obtained parameters for each gate opening (e) and measurement ranges

Table 1. Obtained parameters for each gate opening (e) and measurement ranges								
Gate	Total test	Discharge	Total Head	y1 (cm)	y2 (cm)	Froude		
Opening	number	Range	Range	Range	Range	Num. Range		
e (cm)		Q (lt/s)	H (cm)			\mathbf{F}_{r1}		
e ₁ =2.5	13 Tests	14.70-25.70	13.40-38.90	1.60-1.80	9.10-13.20	3.87-5.66		
$e_2=3.5$	24 Tests	19.85-32.04	13.10-30.80	2.20-2.40	9.50-15.00	3.24-4.59		
e ₃ =4	24 Tests	22.27-34.15	13.10-28.30	2.40-2.50	10.10-15.50	3.19-4.60		
$e_{4}=5$	12 Tests	29.60-41.50	15.60-27.80	3.10-3.80	12.00-15.10	2.89-2.98		
e5=6	23 Tests	35.03-46.90	15.40-25.60	3.60-3.90	12.70-16.50	2.73-3.24		

Since the aim of the study was to determine the location of the hydraulic jump (L), which varying depending on the discharge (Q) and the gate opening (e), the experiments aimed to create a free hydraulic jump in the open channel. For an observable hydraulic jump, the regime of the flow passing under the gate must change from supercritical to subcritical. The regime of the flow passing from under the gate does not changed until the end of the channel unless it encounters an obstacle. In order to provide the flow regime change, a rectangular linear weir with a height of 5 cm was placed at the end of the channel (Figure 6). The Fr varies between 2.7 and 6.8 for subcritical regime. This weir remained as submerged during all experiments, increasing the flow depth and creating the subcritical regime. The linear weir was placed 450 cm far away from the sluice gate.

The total upstream head (H) behind the sluice gate was obtained from the sum of the upstream water depth (h) and the velocity head $(V^2/2 \times g)$. The piezometric depth (h) behind the gate and the velocities used in the velocity head calculations were measured 20 cm behind the sluice gate. Although the upstream side of the gate acts like a reservoir, a swell occurs at a distance of 7-10 cm just behind the gate due to the impact of the flow to the gate. For this swell not to affect the depth measurement, a point 20 cm behind the gate where water surface is flat was selected for the measurements. The velocity measured with an acoustic doppler velocimeter (ADV). Velocity measurements can be made in 3 axes with an ADV, but since the current flows in the +x direction, the velocity values obtained in the +x direction was used in the velocity head $(V^2/2 \times g)$ calculations.

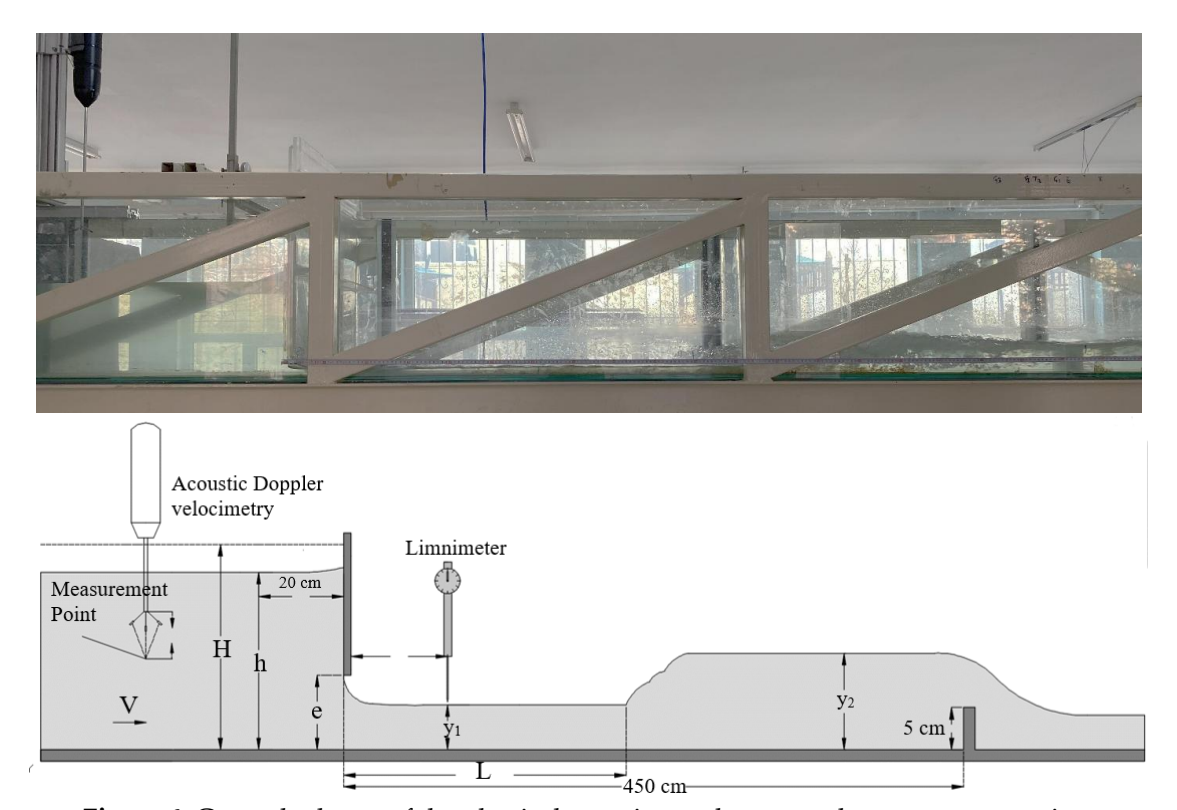


Figure 6. General scheme of the physical experimental setup and measurement points

2.3 Particle Swarm Optimization Algorithm

Particle Swarm Optimization (PSO) algorithm is a heuristic-based optimization algorithm first proposed by Kennedy and Eberhart [29]. In the PSO algorithm, behaviors of birds and fishes for searching food, which are living in a herd in nature are modeled. Due to its simplicity of use and being a successful optimization algorithm, the PSO algorithm has been applied to many engineering problems and successful results have been obtained [30]. In PSO, in the first stage, all particles are randomly distributed in nature and determine the locations of possible food sources in the range of [xjmin; xjmax]. he Z objective function is evaluated at the position of each particle, representing a potential solution point. This evaluation helps determine how good or effective each solution is, allowing the algorithm to assess the quality of the solutions found by the particles. At this stage, the best food location obtained by each particle is recorded as pbest, and the highest quality food location reached by the colony is recorded in the common memory of the colony as gbest. Then, as shown in Equation (4), the speed values that allow each particle to move towards the best results obtained both locally (pbest) and globally (gbest) are calculated. Then, with the help of these values, the position information of the particles is updated as shown in Equation (5).

$$v_{ij}^{t+1} = w v_{ij}^t + c_1 r_1 (p_{best} - X_{ij}) + c_2 r_2 (g_{best} - X_{ij})$$
(4)

$$X_{ij}^{t+1} = X_{ij}^t + v_{ij}^{t+1} (5)$$

The speed value v_{ij}^{t+1} obtained for the solution point X_{ij} is shown in Equation (4). The w value in the equation is the inertia weight which provides the sensitivity of the search, a more global search is performed with large w values, while more local searches are performed with small w values. It is

recommended that the inertia weight to be determined in a way that it decreases linearly throughout the iterations for a more successful solution [31]. The c₁ and c₂ values in Equation (4) are the acceleration coefficients. While c₁ pulls the positions of the particles towards the p_{best} values, c₂ pulls them towards the g_{best} values. Although the acceleration coefficients vary according to the type of problem, the value c₁ = c₂ = 2.0 is generally recommended as a starting point [32], [33]. The r₁ and r₂ values are randomly generated in the range of [0,1] and provide the randomness of the PSO algorithm. After calculating the velocity values of all particles, the new positions of the particles are determined with the help of Equation (5). The Z objective function is run again for the current positions of the particles and the quality of the new solution points obtained is determined. The p_{best} and g_{best} values are updated throughout the iterations and the search process continues.

In the current study, V_1 , H, y_1 and y_2 values be used as model inputs and modeling will be carried out using the PSO algorithm in order to estimate L values. Here, the two most well-known basic modeling types, linear (Equation 6) and nonlinear (Equation 7) model structures, were preferred.

$$L_L = \beta_1 * V_1 + \beta_2 * H + \beta_3 * y_1 + \beta_4 * y_2 \tag{6}$$

$$L_{NL} = V_1^{\beta_1} * H^{\beta_2} * y_1^{\beta_3} * y_2^{\beta_4} \tag{7}$$

The PSO algorithm will be used to determine the β coefficients that will create the most successful modeling at this stage. While designing the algorithm, a limit is determined for the search space of the β coefficients as $[x_i^{min}; x_j^{max}]$ and the best model information is sought within this limit.

While creating models, Z objective functions are used to determine whether any model is better than others. If the L values generated by the developed models are denoted as LML_MLM, and the L value obtained from experimental observations is denoted as LOL_OLO, then the objective functions for the PSO (Particle Swarm Optimization) algorithm can be formulated using various statistical indicators. These indicators measure the difference or error between the model predictions and experimental results, as shown below. Mean Squared Error (MSE) is shown in Equation (8), Coefficient of Determination R^2 is shown in Equation (9) and Nash Sutcliffe Efficiency Coefficient (NSE) is shown in Equation (10). Any of these indicators can be used as an objective function alone or they can be used in proportion to each other as shown in Equation (8). Here, if Z_1 or Z_4 is chosen as the objective function, the optimization problem turns into minimization, and if Z_2 or Z_3 is chosen, it turns into maximization. In the PSO (Particle Swarm Optimization) algorithm, the effectiveness of the model structure generated in each iteration is evaluated based on the chosen objective function, which reflects how well the model's predictions match the actual data. Based on this evaluation, the β coefficients—representing the model parameters—are updated to guide the search toward more accurate and successful models in subsequent iterations. In this way, it is aimed to determine the most successful model structure.

$$Z_1 = MSE = \frac{\sum_{i=1}^{N} (L_O - L_M)^2}{N}$$
 (8)

$$Z_2 = R^2 = \frac{\left[\sum_{i=1}^N (L_O - \overline{L_O})(L_M - \overline{L_M})\right]^2}{\sum_{i=1}^N (L_O - \overline{L_O})^2 \sum_{i=1}^N (L_M - \overline{L_M})^2}$$
(9)

$$Z_3 = NSE = 1 - \frac{\sum_{i=1}^{N} (L_O - L_M)^2}{\sum_{i=1}^{N} (L_O - \overline{L_O})^2}$$
 (10)

$$Z_4 = \frac{MSE}{NSE} \tag{11}$$

3. RESULTS AND DISCUSSION

In the present study, linear and nonlinear models were created as shown in Equation (6) and Equation (7) using the PSO algorithm to estimate hydraulic jump positions (L). For this purpose, the results obtained from a total of 96 experimental measurements were first divided into two group as training and test. While a total of 73 experimental results from experiments with a gate opening (e) of 2.5 cm, 3.5 cm, 4 cm and 5 cm were separated as the training group, 23 experimental results with a gate opening (e) of 6 cm constituted the test group. Models will be created for the training group with the help of the PSO algorithm and these models will be applied to the test group to examine how consistent the model results and the observed experimental results are.

Since there are 4 input parameters in all linear and nonlinear modeling studies with the PSO algorithm, the problems were solved in 4 dimensions. In all studies, the particle number was 8 and The $[x_j^{min}; x_j^{max}]$ interval, which defines the boundaries of the search space, was set to [-5;5]. The inertia weight w was linearly decreased over the iterations within the range [0.9;0.4]. Similarly, the acceleration coefficients $c_1 = c_2 = 2.0$ were accepted and 2000 iterations were performed.

In the search operations performed in the PSO algorithm, the Z_4 objective function shown in Equation (11) is preferred. In this way, the minimization of Z_4 values is aimed. The minimization of Z_4 values aims to minimize the MSE values expressing the error values and to maximize the NSE metric, which is a strong performance indicator at the same time. Since the NSE metric taking values in the range of $[-\infty;1]$ will bring some problems, a manipulation was made in the NSE metric as shown in Equation (12) below.

if
$$NSE \le 0 \to NSE = 10^{-\Delta}$$
; if $NSE > 0 \to NSE = NSE$ (12)

In Equation (12), when the Δ values take large values, the negative NSE values take very low values on the positive side, causing the Z₄ values to increase astronomically, and in this way, the models that produce negative NSE values are naturally eliminated. In this way, the most successful models can be determined among the models that give positive NSE values. The value Δ =11 was used in the current study[34].

In summary, the PSO algorithm searches for the β coefficients shown in Equation (6) and Equation (7) in the range of [-5;5]. It evaluates the model result it produces with the Z₄ objective function. It tries to produce the model information with the lowest Z₄ value by changing the β coefficients throughout the iterations. After the PSO algorithm was designed in this way, 30 linear and 30 nonlinear models were produced. The model information produced and the performance indicators of the models are shown in detail in Appendix A.

As a result of the studies, the most successful model for linear modeling (L_L^{Best}) is shown in Equation (13), and the most successful model for nonlinear modeling (L_{NL}^{Best}) is shown in Equation (14). On the other hand, the statistical indicators of the most successful models obtained are given in Table 2.

$$L_L^{Best} = -2.8591 * V_1 + 0.1202 * H - 1.1007 * y_1 + 0.5733 * y_2$$
(13)

$$L_{NL}^{Best} = V_1^{4.9892} * H^{2.0287} * y_1^{2.2718} * y_2^{-4.3645}$$
(14)

When the results obtained from Table 2 are analyzed, two situations stand out in particular. First, it is seen that the PSO algorithm can achieve quite successful results within the framework of this problem. In both linear and nonlinear modeling, the PSO algorithm has shown a very successful performance. When the test results are examined in particular, a very high value of NSE = 0.954 was reached in linear modeling, while the value of NSE = 0.902 was reached in nonlinear modeling. The fact that the results of both methods are above 0.9 shows that the PSO algorithm is quite successful in this regard when evaluated within the framework of a strong metric such as NSE. The second important result obtained in line with Table 2 is that linear modeling is clearly more successful than nonlinear modeling. More

successful results were obtained with the linear modeling method compared to nonlinear modeling in all evaluation criteria except the test R² metric. Due to the fact that the relationships between the model's input and output parameters tend to exhibit more linear behavior, the linear modeling approach has cumulatively achieved higher performance values in the research results. Although the nonlinear models yielded very high R2 results in the testing phase, they performed worse during training and exhibited higher MSE values. This may indicate overfitting or overly complex model structures.

Table 2. Performance indicators of the most successful solutions obtained.

		Performance Indicators	Linear Modelling (L _L ^{Best})	Nonlinear Modelling (L_{NL}^{Best})
-	8	R^2	0.942	0.653
	піпв	NSE	0.942	0.562

MSE 0.042 0.320 MSE/NSE 0.045 0.569 R^2 0.983 0.990 NSE 0.954 0.902 **MSE** 0.022 0.047

MSE/NSE 0.023 0.052 On the other hand, the minimum, average and maximum values of the performance indicators of the 30 models produced are shown in Table 3 below. As can be understood from Table 3, more successful results were achieved in linear modeling in all evaluation criteria except Test R2. When the average performance values for both modeling methods are examined, while the value of NSE=0.943 was obtained in linear modeling in the training phase, the value of NSE=0.720 was reached in nonlinear modeling. In this respect, approximately 25% more successful results were achieved in linear modeling in the training phase. When the results in the test phase are examined, the average NSE value of 30

models in linear modeling is 0.942, while this value is calculated as 0.807 in nonlinear modeling. In this respect, it can be said that linear modeling is 16.7% more successful in the test results. The same success is also seen in MSE values, which are an error indicator. The MSE values of linear modeling are much lower than nonlinear modeling. In order to visually present the performance of the methods in general, radar diagrams of the evaluation metrics used were created and presented in Figure 7. It can be visually understood that the models produced as a result of linear modeling are more successful.

Table 3. Summary values of the performance of the models produced with the help of the PSO

algorithm.									
		Training			Testing				
		R^2	NSE	MSE	MSE/NSE	R^2	NSE	MSE	<i>MSE/NSE</i>
	Minimum	0.936	0.934	0.041	0.044	0.983	0.924	0.022	0.023
Linear Modelling	Mean	0.943	0.943	0.042	0.045	0.985	0.942	0.028	0.030
	Maximum	0.944	0.944	0.048	0.052	0.987	0.954	0.036	0.039
	Minimum	0.637	0.553	0.142	0.177	0.987	0.748	0.047	0.052
Nonlinear Modelling	Mean	0.750	0.720	0.204	0.291	0.990	0.807	0.093	0.117
	Maximum	0.822	0.805	0.326	0.590	0.990	0.902	0.121	0.162

The findings obtained from the studies were evaluated in terms of the stability of the methods in another stage. For this purpose, the information belonging to the first 10 most successful models obtained as a result of linear [L_L1(Best)-L_L10] and nonlinear [L_{NL}1(Best)-L_{NL}10] modeling was processed into Taylor diagrams and the performances of the methods were evaluated in a different framework. The standard deviation and NSE (or R2) values formed by the models obtained in the Taylor diagrams are processed circularly and angularly, respectively, and interpretations are made based on the positions of the models on the diagram. In Taylor diagrams; if the point where any produced model is marked is

further (angularly) clockwise and closer (circularly) to the observed standard deviation curve, it indicates that the model is more successful, while the opposite indicates that it is a less successful model. The successes of the produced models are shown in Figure 8a for the training stage and in Figure 8b for the testing stage. In order to observe the obtained findings more clearly and understandably, not all models were included in the Taylor diagrams and only the most successful 10 model results were shown. When both Figure 8a and Figure 8b are examined, it is seen that the linear modeling results are very stable and located in a very narrow area. In contrast, the models obtained as a result of nonlinear analysis exhibit a more scattered structure and exhibit lower performance. When the nonlinear analysis results in Figure 8a are examined in particular, it can be seen that the result values are spread over a very wide area. On the other hand, when Figure 8a is examined in particular, it is seen that the results obtained as a result of linear modeling are located very close to the standard deviation curve of the observed data. It is evident that the PSO algorithm can successfully train the model. Furthermore, linear analysis based on Taylor diagrams indicates that more accurate and stable results are achieved.

On the other hand, in order to examine the performances of the most successful models in more detail, the extent to which the two most successful models (L_L^{Best} and L_{NL}^{Best}) produced as a result of linear and nonlinear modeling can capture the observed result values is shown in detail in Figure 9. The ranges of the observed values [-5%; +5%] and [-10%; +10%] were also processed on the same figure and the extent to which the models could enter this range was also examined and the model results were evaluated from a different perspective. The extent to which the L_L^{Best} and L_{NL}^{Best} models could enter the [-5%; +5%] and [-10%; +10%] ranges is shown in detail in Table 4.

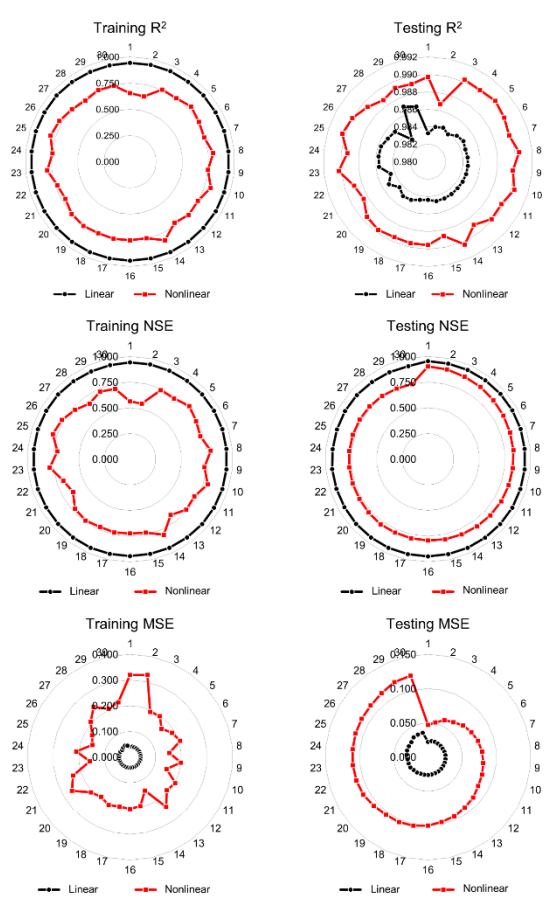


Figure 7. Radar diagrams of the performance of the produced models

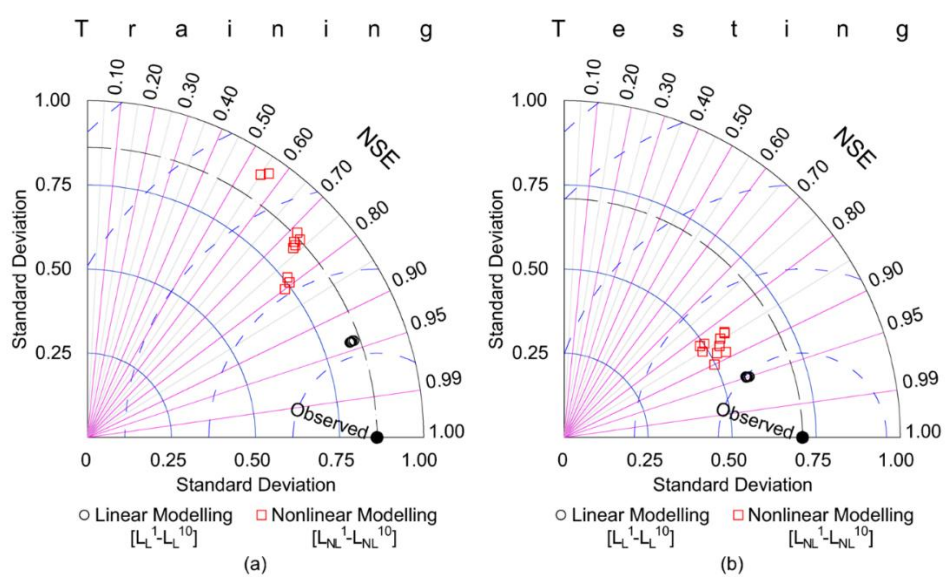


Figure 8. Taylor diagrams for the training (a) and test (b) groups of the top 10 most successful models obtained.

When Figure 9 is examined in general, it can be stated that the L_LBest model was able to capture the experimental results observed in the training phase quite successfully. Especially in the experimental results with a gate opening of e=4 cm in Figure 9a, this model exhibited near-perfect behavior. On the other hand, when the test results in Figure 9b are examined, it can be said that this model is quite successful. When the information shown in Table 4 is examined, the L_LBest model was able to produce values in the [-10%; +10%] range in 47 of the 73 experimental results observed in the training phase. On the other hand, the L_{NL}Best model was able to produce values in the [-10%; +10%] range in only 17 of the 73 experimental results. In other words, while the success rate of the L_LBest model in the [-10%; +10%] range was approximately 64%, the success of the L_{NL}Best model remained at approximately 23%. Model successes for the test phase and the [-5%; +5%] ranges are shown in Table 4. It is seen that linear modeling can capture the observed experimental results more successfully compared to nonlinear modeling.

Up to this stage, it is seen that linear modeling is more successful in terms of performance, stability of the methods and the ability of the methods to capture the observed experimental results and that the PSO algorithm generally produces successful results. After this stage, as a result of the studies carried out, the β values produced by the methods were evaluated within the framework of the parameter effect. For this purpose, BoxPlot diagrams of the β values of 30 models obtained because of linear and nonlinear modeling were created and shown in Figure 10a for linear modeling and in Figure 10b for nonlinear modeling. When Figure 10a is examined, it is clearly seen that the β coefficients form a certain form as a result of linear modeling. In this direction, it is seen that especially β_1 and β_3 are in the negative direction and β_2 and β_4 are in the positive side.

Table 4. The capturing rates of the most successful linear and nonlinear models for different ranges of observation values.

	Train	ing	Testing		
	Range [-10%;+10%]	Range [-5%;+5%]	Range [-10%;+10%]	Range [-5%;+5%]	
$Linear$ (L_{L}^{Best})	<i>47/73 (≈64%)</i>	34/73 (≈47%)	<i>15/23 (≈65%)</i>	12/23 (≈52%)	
Nonlinear (L _{NL} Best)	17/73 (≈23%)	12/73 (≈16%)	14/23 (≈61%)	10/23 (≈44%)	

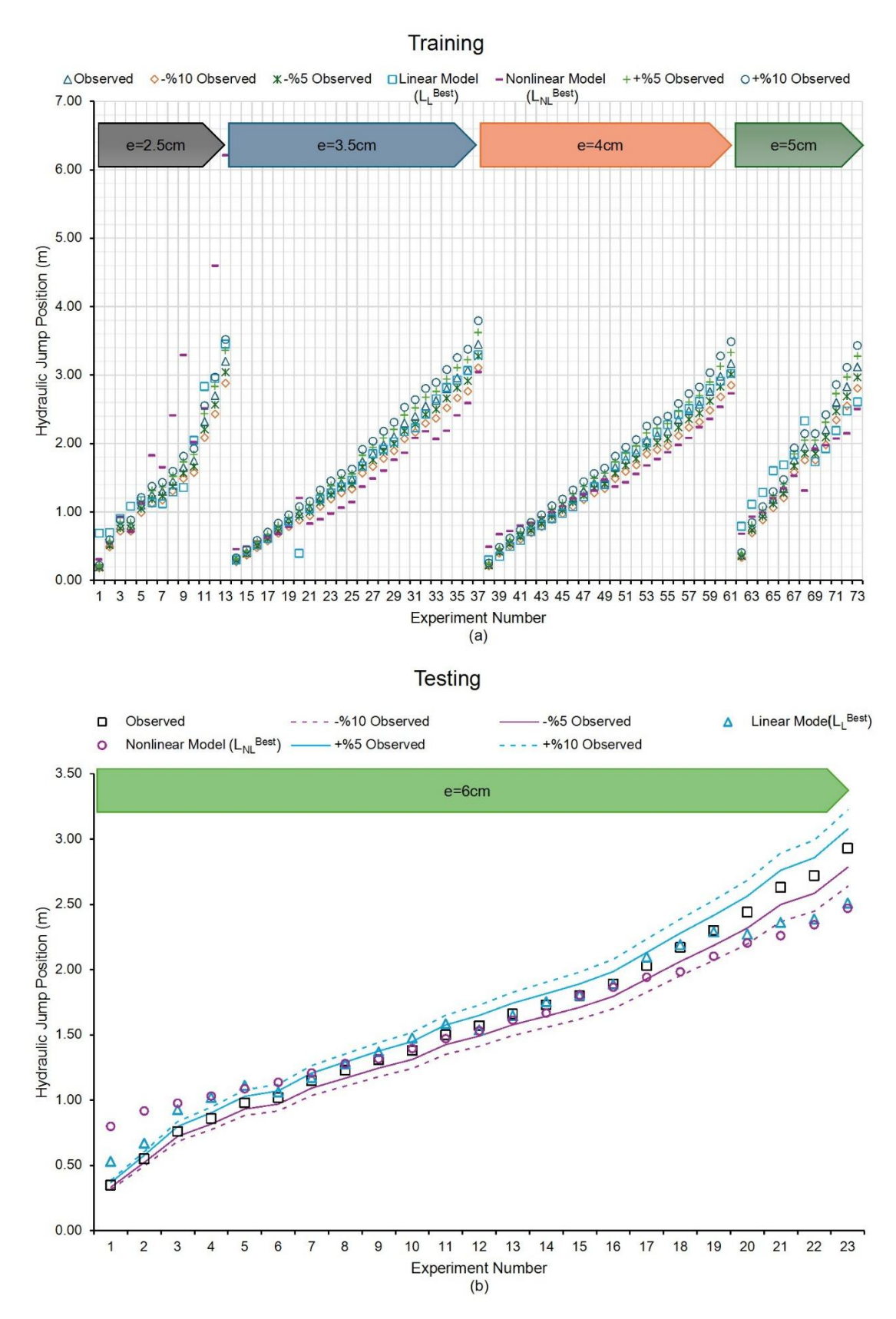


Figure 9. Comparison of the results of the most successful models in the training (a) and testing (b) stages with the observation values.

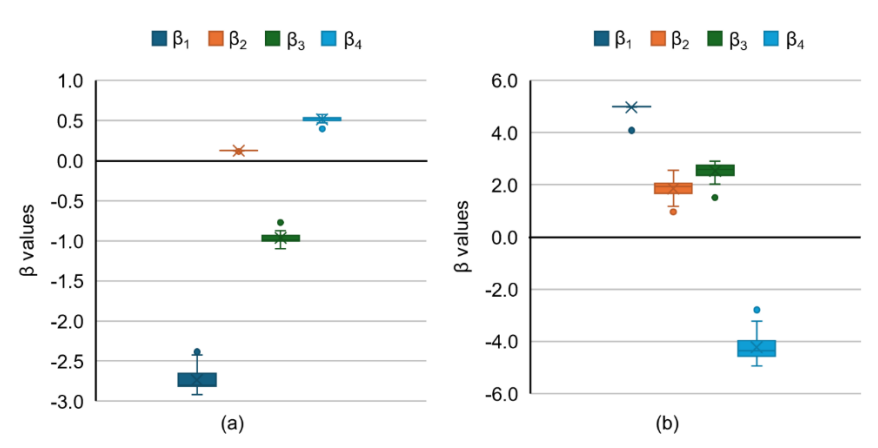


Figure 10. Box plot diagram of β values obtained as a result of linear (a) and nonlinear (b) modeling.

When the basic linear equation model shown in Equation (6) and Figure 10a are examined together, it is understood that the H and y_2 parameters have a significant positive effect on the location of the hydraulic jump (L), while the V_1 and y_1 parameters have a negative effect. The terms "positive" and "negative" effect refer to the direction of influence that independent variables (H, y_2 , V_1 , y_1) have on the dependent variable (L). More specifically, an independent variable with a positive effect increases the value of the dependent variable as it increases. In other words, when H or y_2 increases, the location of the hydraulic jump moves further downstream, and the length L increases. Conversely, an independent variable with a negative effect causes the dependent variable to decrease as it increases. That is, when V1 or y1 increases, the hydraulic jump occurs closer upstream, and the length L decreases.

In line with these results, it is expected result that the H parameter, in particular, remained on the positive side and had a positive effect on the location of the hydraulic jump (L). On the other hand, the fact that both the V_1 and y_1 parameters are in the same direction in a common way leads to the conclusion that the gate opening (e) is a very important parameter on the location of the hydraulic jump (L). It can be said that the gate opening (e) and the upstream total head (H) are one of the basic dynamics determining the location of the hydraulic jump (L).

It is seen that β_1 , the coefficient of the parameter V_1 obtained from the linear equation in Figure 10a, takes a negative value in the linear modeling. The hydraulic jump position (L) moves forward in the open channel with the increasing velocity value (V_1) for all gate openings (e). Therefore, a directly proportional increase between the hydraulic jump position (L) and the velocity values (V_1), i.e. the parameter β_1 , is expected to be positive. The negative value of β_1 , which is the coefficient of velocity value (V_1), is because the upstream total head (H) has a more dominant effect on the hydraulic jump position than the velocity value (V_1). The velocity value (V_1) varies depending on the upstream total head (H) and the gate opening (e). The hydraulic jump was formed by the flow from under a gate in the supercritical regime and the parameters of the entire system were considered. The upstream total head (H) represents the system's total potential energy, which governs all flow characteristics, including the velocity (V_1). As H increases, both the potential energy and its transformation into kinetic energy also rise. Consequently, H becomes the primary determinant not only for V_1 but also for the depth before the jump (V_1) and the hydraulic jump location (L). The strong correlation between H and V_1 diminishes the independent influence of V_1 in the modeling process.

In nonlinear modeling, the coefficient β_1 of the velocity value (V₁) is calculated as positive in contrast to linear modeling. This is due to the difference in the operation of the algorithms of the models. In nonlinear modeling, the flow depth after the jump (y₂) coefficient β_4 was calculated as negative. On the other hand, it is seen that the β_3 and β_4 parameters changed direction in both methods. During the experiments, a significant positive relationship was observed between the y₂ parameter affected by the β_4 coefficient and the location of the hydraulic jump (L). The negative β_4 coefficient is due to the dominance of other experimental parameters, similar to the situation in the linear equation. For these

reasons, it can be said that the information in Figure 10b cannot successfully express the observed results. Based on this, it was concluded that linear modeling was more successful.

4. CONCLUSIONS

The hydraulic jump formed by a flow passing under the gate in supercritical condition was modeled with the Particle Swarm Optimization (PSO) algorithm to determine the location of the jump in open channel. Linear and nonlinear PSO models were created, and it is known that the models created in the studies conducted in the field of applied hydraulics are generally nonlinear. In line with the findings obtained from this study, it was observed that the optimization model established in a linear manner was more successful. PSO algorithm solved the problem more successfully with linear modeling than with nonlinear modeling. It is thought that the change in β coefficients, especially in nonlinear modeling, changes the result significantly, therefore the PSO algorithm cannot achieve more successful results. When the experimental results are examined, the hydraulic jump location (L) moves to downstream within direct proportion with upstream total head (H), velocity (V1), flow depth before jump (y1) and after jump (y2). As expected in linear modeling, the hydraulic jump position (L) does not increase proportionally with all parameters, and the parameters β_1 and β_3 , which belong to the velocity (V₁) and flow depth before jump (y1), are negative in the equation. This is due to the fact that the upstream total head (H) and flow depth after jump (y2) have a more dominant effect on the hydraulic jump position (L). Depending on the type of system, the dominant parameters may affect the jump position more than the other parameters.

Declaration of Ethical Standards

The authors declare that all ethical guidelines including authorship, citation, data reporting, and publishing original research are followed.

Credit Authorship Contribution Statement

- Ali YILDIZ: Conceptualization, Data curation Methodology, Writing original draft, Writing Review and Editing
- Volkan YILMAZ: Formal analysis, Visualization, Writing original draft, Writing Review and Editing

Declaration of Competing Interest

The authors declare that there is no conflict of interest

Funding / Acknowledgements

No Funding is received by authors.

Data Availability

The data that support the findings of this study are available from the corresponding author upon reasonable request.

REFERENCES

[1] K. Safranez, "Researches relating to the hydraulic jump," English translation by DP Barnes, Bureau of Reclamation Files, Denver, CO, USA, File no. 37, 1929.

- [2] A. J. Peterka, "Hydraulic Design of Stilling Basins and Energy Dissipators," 8th ed., Engineering Monograph No. 25, United States Department of the Interior, Bureau of Reclamation, Denver, CO, USA, 1984.
- [3] J. N. Bradley and A. J. Peterka, "Hydraulic Design of Stilling Basins: Hydraulic Jumps on a Horizontal Apron (Basin I)," *Journal of the Hydraulics Division*, vol. 83, no. 5, pp. 1401–1, Oct. 1957, doi: 10.1061/JYCEAJ.0000126.
- [4] W. H. Hager, *Energy Dissipators and Hydraulic Jump*, Water Science and Technology Library, vol. 8. Dordrecht, Netherlands: Springer, 1992.
- [5] U.S. Bureau of Reclamation, *Design of Small Dams*, 2nd ed. Washington, DC, USA: U.S. Government Printing Office, 1977.
- [6] B. A. Bakhmeteff and A. E. Matzke, "The Hydraulic Jump in Terms of Dynamic Similarity," *Transactions of the American Society of Civil Engineers*, vol. 101, no. 1, pp. 630–647, Jan. 1936, doi: 10.1061/TACEAT.0004708.
- [7] M. Cihan Aydın and A. E. Ulu, "Journal of Science and Technology Numerical modelling of sluice gates with different baffle types under submerged flow conditions," *Bitlis Eren University Journal of Science and Technology*, vol. 7, no. 1, pp. 1–6, 2017.
- [8] G. Bidone, "Observations sur la hauteur du ressaut hydraulique en 1818," report presented to the Academy of Sciences of Turin (in French), Turin, Italy, 1819.
- [9] J.-B. Bélanger, Essai sur la solution numérique de quelques problèmes relatifs au mouvement permanent des eaux courantes. Paris, France: École Royale des Ponts et Chaussées, 1828.
- [10] A. G. Levy, J. W. Ellms, W. Gore, ve A. L. Fales, "The hydraulic jump as a mixing device," *Journal of the American Water Works Association*, cilt 17, sayı 1, s. 1–26, 1927, doi:10.1002/j.1551-8833.1927.tb12673.x.
- [11] H. Rouse, T. T. Siao, and S. Nagaratnam, "Turbulence Characteristics of the Hydraulic Jump," *Transactions of the American Society of Civil Engineers*, vol. 124, no. 1, pp. 926–950, Jan. 1959, doi: 10.1061/TACEAT.0007738.
- [12] R. Silvester, "Hydraulic Jump in All Shapes of Horizontal Channels," *Journal of the Hydraulics Division*, vol. 90, no. 1, pp. 23–55, Jan. 1964, doi: 10.1061/JYCEAJ.0000977.
- [13] N. Rajaratnam and K. Subramanya, "Profile of the Hydraulic Jump," *Journal of the Hydraulics Division*, vol. 94, no. 3, pp. 663–674, May 1968, doi: 10.1061/JYCEAJ.0001810.
- [14] W. H. Hager and R. Wanoschek, "Hydraulic jump in triangular channel," *Journal of Hydraulic Research*, vol. 25, no. 5, pp. 549–564, 1987, doi: 10.1080/00221688709499255.
- [15] B. M. Araz Gharangik and M. Hanif Chaudhry, "Numerical Simulation of Hydraulic Jump," *Journal of Hydraulic Engineering*, vol. 117, no. 9, pp. 1195–1211, Sep. 1991, doi: 10.1061/(ASCE)0733-9429(1991)117:9(1195).
- [16] S. A. Ead, M. Asce, N. Rajaratnam, and F. Asce, "Hydraulic Jumps on Corrugated Beds," *Journal of Hydraulic Engineering*, vol. 128, no. 7, pp. 656–663, Jul. 2002, doi: 10.1061/(ASCE)0733-9429(2002)128:7(656).
- [17] A. Habibzadeh, A. R. Vatankhah, and N. Rajaratnam, "Role of Energy Loss on Discharge Characteristics of Sluice Gates," *Journal of Hydraulic Engineering*, vol. 137, no. 9, pp. 1079–1084, Sep. 2011, doi: 10.1061/(ASCE)HY.1943-7900.0000406
- [18] Y. Kim, G. Choi, H. Park, and S. Byeon, "Hydraulic Jump and Energy Dissipation with Sluice Gate," *Water 2015, Vol. 7, Pages 5115-5133*, vol. 7, no. 9, pp. 5115–5133, Sep. 2015, doi: 10.3390/W7095115.
- [19] S. A. M. Movahed, J. Mozaffari, D. Davoodmaghami, and M. Akbari, "A Semi-Analytical Equation to Estimate Hydraulic Jump Length," *Periodica Polytechnica Civil Engineering*, vol. 62, no. 4, pp. 1001–1006, Sep. 2018, doi: 10.3311/PPCI.11257.

[20] O. Simsek, M. S. Akoz, and N. G. S. Oksal, "Experimental analysis of hydraulic jump at high froude numbers," *Sadhana - Academy Proceedings in Engineering Sciences*, vol. 48, no. 2, pp. 1–16, Jun. 2023, doi: 10.1007/S12046-023-02081-8/FIGURES/19.

- [21] M. Naseri and F. Othman, "Determination of the length of hydraulic jumps using artificial neural networks," *Advances in Engineering Software*, vol. 48, no. 1, pp. 27–31, Jun. 2012, doi: 10.1016/J.ADVENGSOFT.2012.01.003.
- [22] M. H. Omid, M. Omid, and M. E. Varaki, "Modelling hydraulic jumps with artificial neural networks," https://doi.org/10.1680/wama.2005.158.2.65, vol. 158, no. 2, pp. 65–70, May 2015, doi: 10.1680/WAMA.2005.158.2.65.
- [23] M. Karbasi and H. M. Azamathulla, "GEP to predict characteristics of a hydraulic jump over a rough bed," *KSCE Journal of Civil Engineering*, vol. 20, no. 7, pp. 3006–3011, Nov. 2016, doi: 10.1007/S12205-016-0821-X/METRICS.
- [24] M. Karbasi, "Estimation of classical hydraulic jump length using teaching–learning based optimization algorithm," *Journal of Materials and Environmental Science*, vol. 7, no. 8, pp. 2947–2954, 2016.
- [25] E. Gul, O. F. Dursun, and A. Mohammadian, "Experimental study and modeling of hydraulic jump for a suddenly expanding stilling basin using different hybrid algorithms," *Water Supply*, vol. 21, no. 7, pp. 3752–3771, Nov. 2021, doi: 10.2166/WS.2021.139.
- [26] A. Yıldız, "Bent Kapağı Altından Geçen Akımın Oluşturduğu Hidrolik Sıçramanın Konumunun Deneysel ve Nümerik Olarak Belirlenmesi," *Black Sea Journal of Engineering and Science*, vol. 7, no. 5, pp. 988–1000, Sep. 2024, doi: 10.34248/BSENGINEERING.1463296.
- [27] P. K. Swamee, "SluiceGate Discharge Equations," *Journal of Irrigation and Drainage Engineering*, vol. 118, no. 1, pp. 56–60, Jan. 1992, doi: 10.1061/(ASCE)0733-9437(1992)118:1(56).
- [28] E. Kubrak, J. Kubrak, A. Kiczko, and M. Kubrak, "Flow Measurements Using a Sluice Gate; Analysis of Applicability," *Water 2020, Vol. 12, Page 819*, vol. 12, no. 3, p. 819, Mar. 2020, doi: 10.3390/W12030819.
- [29] J. Kennedy and R. Eberhart, "Particle swarm optimization," *Proceedings of ICNN'95 International Conference on Neural Networks*, vol. 4, pp. 1942–1948, 1995, doi: 10.1109/ICNN.1995.488968.
- [30] X. Li and S. Li, "An adaptive surrogate-assisted particle swarm optimization for expensive problems," *Soft comput*, vol. 25, no. 24, pp. 15051–15065, Dec. 2021, doi: 10.1007/S00500-021-06348-2/TABLES/6.
- [31] Y. Shi and R. C. Eberhart, "Empirical study of particle swarm optimization," *Proceedings of the 1999 Congress on Evolutionary Computation, CEC 1999*, vol. 3, pp. 1945–1950, 1999, doi: 10.1109/CEC.1999.785511.
- [32] E. Ozcan and C. K. Mohan, "Particle swarm optimization: Surfing the waves," *Proceedings of the 1999 Congress on Evolutionary Computation, CEC 1999*, vol. 3, pp. 1939–1944, 1999, doi: 10.1109/CEC.1999.785510.
- [33] R. C. Eberhart and Y. Shi, "Particle swarm optimization: Developments, applications and resources," *Proceedings of the IEEE Conference on Evolutionary Computation, ICEC*, vol. 1, pp. 81–86, 2001, doi: 10.1109/CEC.2001.934374.
- [34] D. N. Moriasi, J. G. Arnold, M. W. Van Liew, R. L. Bingner, R. D. Harmel, and T. L. Veith, "Model Evaluation Guidelines for Systematic Quantification of Accuracy in Watershed Simulations," *Trans ASABE*, vol. 50, no. 3, pp. 885–900, 2007, doi: 10.13031/2013.23153.